PHOTONICS Research

Directly modulated quantum dot lasers on silicon with a milliampere threshold and high temperature stability

Yating Wan,[1,†,*] Daisuke Inoue,[1,2,†] Daehwan Jung,[1,†] Justin C. Norman,[3] Chen Shang,[3] Arthur C. Gossard,[3,4] and John E. Bowers[3,4]

[1]Institute for Energy Efficiency, University of California Santa Barbara, Santa Barbara, California 93106, USA
[2]Institute of Innovative Research, Tokyo Institute of Technology, Tokyo 152-8552, Japan
[3]Materials Department, University of California Santa Barbara, Santa Barbara, California 93106, USA
[4]Department of Electrical and Computer Engineering, University of California Santa Barbara, Santa Barbara, California 93106, USA
*Corresponding author: yatingwan@ucsb.edu

Received 13 April 2018; revised 5 June 2018; accepted 6 June 2018; posted 7 June 2018 (Doc. ID 328267); published 10 July 2018

Microring lasers feature ultralow thresholds and inherent wavelength-division multiplexing functionalities, offering an attractive approach to miniaturizing photonics in a compact area. Here, we present static and dynamic properties of microring quantum dot lasers grown directly on exact (001) GaP/Si. Effectively, a single-mode operation was observed at 1.3 μm with modes at spectrally distant locations. High temperature stability with T_0~103 K has been achieved with a low threshold of 3 mA for microrings with an outer ring radius of 15 μm and a ring waveguide width of 4 μm. Small signal modulation responses were measured for the first time for the microrings directly grown on silicon, and a 3 dB bandwidth of 6.5 GHz was achieved for a larger ring with an outer ring radius of 50 μm and a ring waveguide width of 4 μm. The directly modulated microring laser, monolithically integrated on a silicon substrate, can incur minimal real estate cost while offering full photonic functionality.

OCIS codes: (230.5590) Quantum-well, -wire and -dot devices; (250.5960) Semiconductor lasers; (160.3130) Integrated optics materials; (140.3945) Microcavities.

https://doi.org/10.1364/PRJ.6.000776

1. INTRODUCTION

Recent years have witnessed significant progress in making ever smaller and more efficient lasers [1–9]. Lasing in quantum dot (QD) microcavity structures has opened a new paradigm that allows exceptional lasing performance, even for lattice-mismatched material systems [10,11]. The discrete number of modes and small volume of the microlasers allow ultralow threshold lasing down to milliampere values [12]. The carrier localization enabled by QDs provides a notable advantage in scaling to small dimensions through reduced sidewall recombination [13]. The use of QDs over quantum wells as a gain medium for silicon (Si) photonics is further motivated by the quest for reduced sensitivity to dislocations generated by heteroepitaxy [14–16]. Such epitaxial approaches not only provide a lower barrier to entry for Si photonics devices through larger substrate growth, but also benefit from the inherent high temperature stability and low threshold lasing characteristics of QD devices, compared to quantum well counterparts [17–19]. Great progress has been made in the field of heteroepitaxial growth of QD-on-Si lasers with reliable, continuous-wave (CW) operation [20–27]. By employing an on-axis (001) GaP/Si substrate using molecular beam epitaxy (MBE), record setting Fabry–Perot lasers have been achieved with low threshold current densities of 132 A/cm^2, and single-side output powers of 175 mW at room temperature under CW operation [27]. However, these edge-emitting laser structures have large footprints of hundreds of square micrometers and power consumptions of several picojoules per bit. Such sizes are orders of magnitude too large to be viable for integration with electronic integrated circuits. Proportional to the active volume of the lasers, the power consumption of such devices is also orders of magnitude higher than that required for on-chip optical interconnects, where the complete energy budget for an optical link should be only about 10 fJ per bit [28].

In this paper, we report whispering gallery mode (WGM) cavity microring lasers on (001) GaP/Si substrate for easily manufacturable on-chip Si light sources with dense integration and low power consumption. A p-doped active region was adopted to improve temperature stability [29] and to suppress gain saturation [30]. A maximum lasing temperature of 80°C

under CW injection has been achieved while maintaining a low threshold of 3 mA. This vastly surpasses the performance of prior lasers with undoped active regions [31,32]. The hole concentration of 5×10^{17} cm^{-3} from p-doping in the barriers also suppresses hole depletion and improves the carrier transport to the dot active layers [30,33]. Small signal modulation responses were measured for the first time for the microrings directly grown on Si, and a 3 dB bandwidth of 6.5 GHz is reported here.

2. EXPERIMENTS AND RESULTS

The complete epitaxial structure is shown in Fig. 1. The detailed growth procedure on the crystalline (001) GaP/Si substrate was reported in Ref. [34]. Two GaAs/$Al_xGa_{1-x}As$ graded index separate confinement heterostructure (GRINSCH) lasers with seven layers of InAs/InGaAs QD-in-a-well (DWELL) active layers were grown on such substrates. A dot density of 5.2×10^{10} cm^{-2} was measured using atomic force microscopy (AFM) and a strong luminescence at 1285 nm with a full width at half-maximum of 28 meV was obtained from photoluminescence measurements. In one laser, the GaAs barriers separating the QDs were partially p-modulation-doped with beryllium (The p-doping density is 5×10^{17} cm^{-3}. The hole sheet density is 5×10^{11} cm^{-2} considering the p-GaAs layer thickness of 10 nm. The hole density per QD is 10) [35]. Otherwise, the two structures are nominally the same.

Ring resonators with varying radii and ring waveguide widths were fabricated from the as-grown materials [22]. A schematic of the device structure is presented in Fig. 2(a). We used an i-line (365 nm) step-and-repeat exposure tool for lithographic patterning to provide high resolution and critical alignment for definition of the electrode metallization in the microsized cavity. The laser cavity was patterned into deeply etched rings to provide strong index guiding of the optical mode as well as suppression of current spreading. A scanning electron microscope (SEM) image of the fabricated device is presented in Fig. 2(b). The devices were then placed and probed on a copper heat sink. An infrared image of a microring laser operated above threshold is shown in Fig. 2(c). All laser measurements presented here were conducted in CW mode.

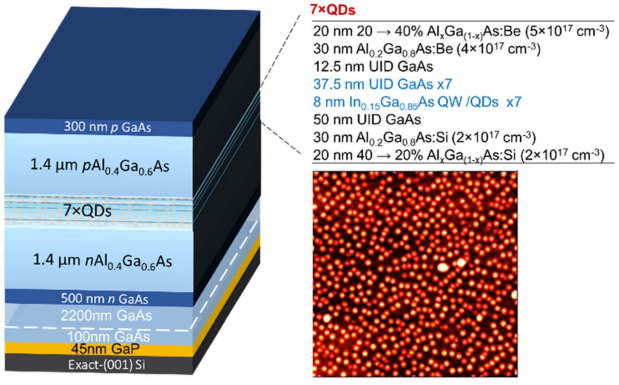

Fig. 1. Schematic of the epilayer structure. Inset, AFM morphology of the uncapped dots.

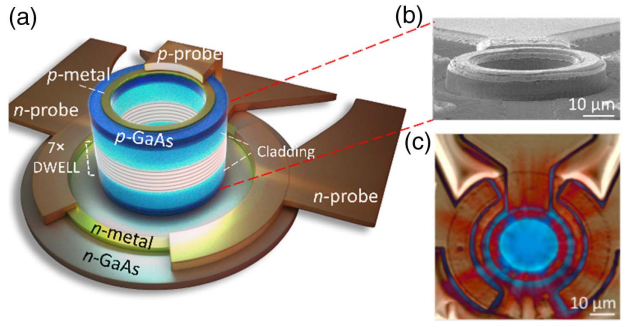

Fig. 2. (a) Schematic illustration and (b) tilted SEM image of one fabricated microring laser; (c) top view of the probed microring under infrared imaging.

A. Static Characteristics

We first injected a direct current (dc) into the device and measured the laser characteristics at room temperature. The light-current-voltage (*L-I-V*) curve of an undoped microring laser with an outer ring radius (R) of 15 μm and a ring waveguide width (W) of 4 μm is shown in Fig. 3. CW thresholds as low as 3 mA were measured, as shown in the inset in Fig. 3.

Figure 4 shows the lasing spectra of this ring resonator with increasing injection current. Bright and clearly defined cavity mode peaks, well above the background QD emission in the O-band, were observed. An excellent extinction ratio over 30 dB for primary lasing mode and good side-mode suppression ratio of 16 dB can be achieved at certain injection levels (20–25 mA in this case). More consistent single-wavelength lasing was observed in smaller diameter devices with larger free spectral range (FSR).

The same microring laser was tested at various heat sink temperatures and its *L-I* characteristic was analyzed in Fig. 5(a). CW lasing was observed up to 40°C, and a characteristic temperature T_0 was extracted to be around 22 K through linear fitting [blue dotted lines in Fig. 5(c)]. The relatively low value of T_0 was partially attributed to self-heating effects and carrier leakage of the undoped active region under CW excitation. Similar *L-I-V* characteristics are obtained for the same

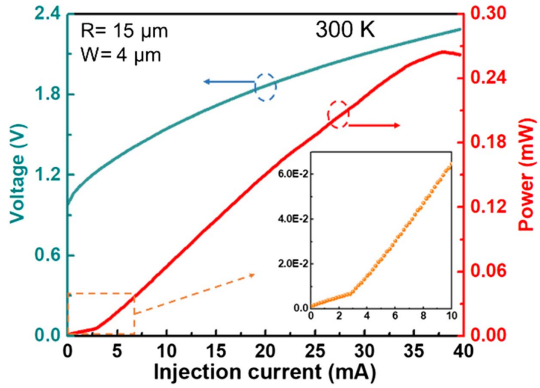

Fig. 3. Measured *L-I-V* curve of a microring laser with intrinsic active region. The device features an outer ring radius of 15 μm and a ring waveguide width of 4 μm. Inset, zoomed-in view of the *L-I* curve in the low-injection region.

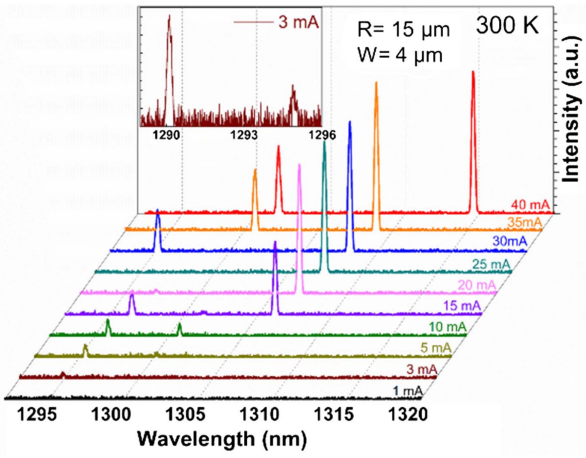

Fig. 4. Emission spectra for the same device in Fig. 3 at various injection currents under CW operation at room temperature. Inset, emission spectrum around lasing threshold.

nominal laser structure grown on a separate wafer but with modulation p-doped active regions. Measured *L-I* curves as a function of the heat sink temperature were plotted in Fig. 5(b). The red dots and line in Fig. 5(c) show the threshold versus temperature curve and fitting. Compared with the undoped device in Fig. 3(a), CW lasing temperature was elevated up to 80°C. An excellent T_0 was extracted to be ~103 K near room temperature (20°C–40°C), and ~35 K between 40°C and 80°C under CW excitation. The dramatically improved high temperature performance with p-doped active region stems from the compensation for the thermal excitation of holes in the lasing mode at higher temperatures [29].

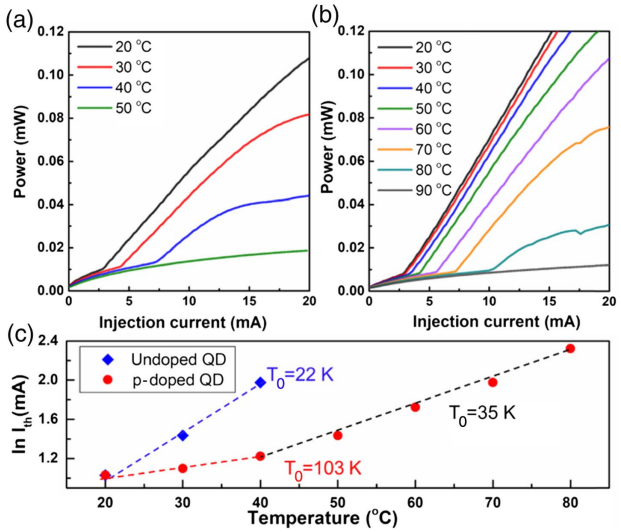

Fig. 5. Measured *L-I* curves as a function of the heat sink temperature for two microring lasers with (a) an intrinsic active region and (b) a modulation p-doped active region. Both devices have an outer ring radius of 15 μm and a ring waveguide width of 4 μm. (c) Temperature-dependent threshold current versus heat sink temperature for the two microring lasers, where the dashed lines represent the linear fit to the experimental data.

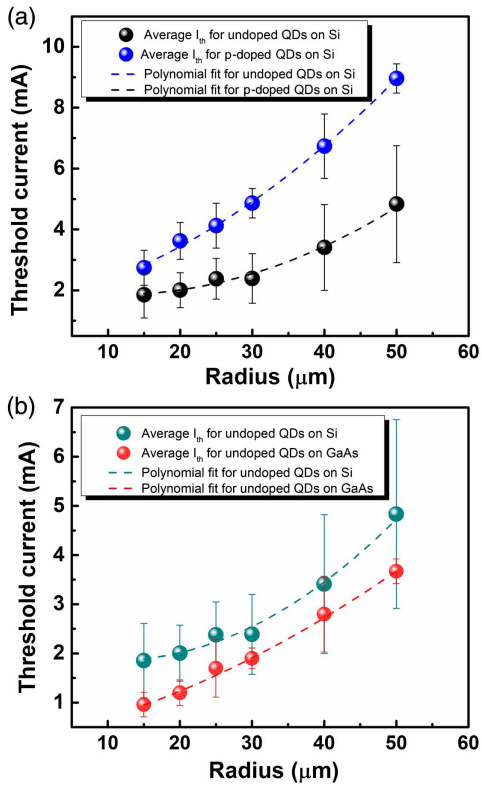

Fig. 6. Threshold currents as a function of outer ring radius for microring lasers (a) with an intrinsic active region and a modulation p-doped active region on the GaP/Si, and (b) on GaP/Si substrate and native GaAs substrate with an intrinsic active region.

Figure 6 summarizes the threshold currents obtained from a series of microring lasers with different outer-ring radii and a constant-ring waveguide width of 4 μm. In Fig. 6(a), devices with intrinsic active region (black) possess average thresholds in the range of 1.8–4.8 mA, roughly 2 times lower than from devices with a modulation p-doped active region (blue), where the average thresholds fall into the range of 2.7–8.9 mA. The threshold current was monotonically decreased with reduction of the ring diameter in both kinds of devices. This further features the carrier localization capability of QDs that enables device miniaturization without imposing a heavy penalty on the threshold current of laser devices [14]. In Fig. 6(b), devices grown on GaP/Si template and native GaAs substrates were compared to evaluate the effect of dislocations on the device performance. Both devices have an intrinsic active region. Around 2–3 times higher threshold current for devices with the same dimension was observed on the GaP/Si templates compared to that on the native substrate, which originates from nonradiative recombination. Better intrinsic performance of the heteroepitaxially grown lasers could be achieved by reducing nonradiative losses via enhancing the quality of the GaAs films on Si.

B. Dynamic Characteristics

A low fiber coupling output power prevents us from performing the signal response of the small size of lasers at this time, due to the large coupling loss between the device and the fiber.

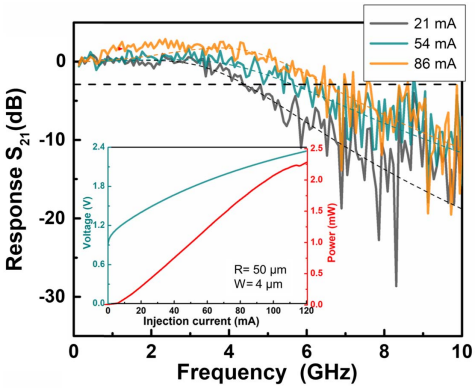

Fig. 7. Small-signal modulation responses of the QD ring laser biased from 21 to 86 mA. The fitting curves are drawn using a three-pole fitting function $H(f)$. Inset, L-I-V characteristics from the same device.

The small-signal response, S_{21}, was measured with a larger device with an outer ring radius of 50 μm and a ring waveguide width of 4 μm, using a 20 GHz light wave component analyzer (LCA, HP8703A).

The devices were directly probed using a signal/ground (SG) radio frequency (RF) probe. No temperature control was applied. Figure 7 shows small-signal modulation response S_{21} of the device, and the inset in Fig. 7 shows the corresponding L-I-V characteristics. The injected currents were varied from 21 to 86 mA. These responses are normalized at low frequency, and a 3 dB bandwidth of 6.5 GHz was attained at a bias current of 86 mA. The responses were further fit using a three-pole fitting function $H(f)$ [36]. The fitted curves are presented in the dashed lines in Fig. 7.

The damping rate γ and relaxation oscillation frequency f_r at each bias current were extracted. The extracted f_r, together with the measured $f_{3\,\mathrm{dB}}$ are plotted in Fig. 8 as a function of the square root of bias current above threshold. The modulation efficiencies of 0.38 GHz/mA$^{1/2}$ for $f_{3\,\mathrm{dB}}$ and 0.34 GHz/mA$^{1/2}$ for f_r were extracted by linear fitting, using the data points below $(I_b - I_{\mathrm{th}})^{1/2} = 8$ mA$^{1/2}$. By linear fitting the damping rate γ versus squared f_r, shown in the inset

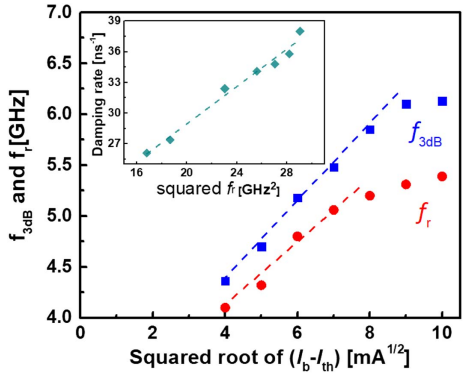

Fig. 8. 3 dB bandwidth $f_{3\,\mathrm{dB}}$ and relaxation oscillation frequency f_r versus square root of the bias current above threshold. Inset, damping rate γ versus squared relaxation oscillation frequency f_r. The maximum 3 dB bandwidth limited by K-factor $f_{3\,\mathrm{dB,\,max}}$ is 9.7 GHz.

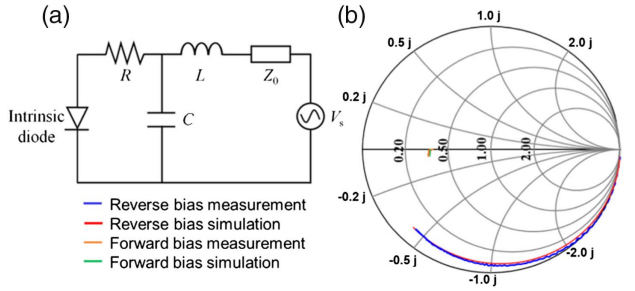

Fig. 9. (a) Impedance measurement of QD microring laser on Si; (b) equivalent circuit model used for the fitting. Measured and fitted curves of reflection S_{11} characteristics for reverse (−3 V) and forward (50 mA) biased condition from 0.14 to 5 GHz.

in Fig. 8, the K-factor is 0.91 ns, and a maximum K-factor limited $f_{3\,\mathrm{dB,\,max}}$, was calculated to be 9.7 GHz using the equation [37]

$$\gamma = K \cdot f_r^2 + \gamma_0, \tag{1}$$

where γ_0 represents the damping offset.

Since the maximum $f_{3\,\mathrm{dB,\,max}}$ is calculated to be 9.7 GHz, smaller than the measured $f_{3\,\mathrm{dB}}$ of 6.5 GHz from the small-signal modulation, the first assumption is due to the large pad capacitance of the electrodes, which are not optimized for high-frequency operation. To better understand how the extrinsic electrical properties of the QD microring lasers affect their modulation bandwidth, we then measured and analyzed the reflection coefficient S_{11} to extract the impedance and estimate the resistor–capacitor (RC) cutoff frequency. The equivalent circuit model [38] used for the fitting is shown in Fig. 9(a). The model consists of an inductance L, a total capacitance C (parasitic capacitance between the contact pads and junction capacitance of the laser diode), a device resistance R, a characteristic impedance of the transmission line (50 Ω) Z_0, and a voltage source V_s. Figure 9(b) shows 50-Ω normalized Smith chart of S_{11} characteristics of the QD ring laser. Reverse (−3 V) and forward (50 mA) biased conditions were applied, respectively. The S_{11} data were fit to the circuit model to obtain the circuit capacitances and resistances. The total capacitance was extracted to be 0.74 pF. The pad capacitance was estimated to be 0.33 pF by approximating the p-probe pad area with 80-μm width and 120-μm length over a 1-μm-thick SiO_2 layer (RF dielectric constant $\varepsilon = 3.9$). The inductance L was negligibly small, as the electrical contact was performed by an RF probe without any wire bonding. Using the obtained circuit parameters ($C = 0.74$ pF, $R = 20.9\,\Omega$), the RC cutoff frequency is calculated to be 10.3 GHz. To further improve the bandwidth, the pad capacitance can be reduced by depositing the metals on a several micron-thick benzocyclobutene (BCB, $\varepsilon = 2.6$) layer. Moreover, the dot density can be increased to enhance the differential gain [39], and a graded p-modulation doping could improve the carrier transport further [40].

3. CONCLUSION

In conclusion, we characterize the lasing performance for QD microlasers grown on exact (001) GaP/Si under electrical

injection. CW thresholds as low as 3 mA and high temperature operation up to 90°C were simultaneously achieved for small footprint ring resonators with an outer ring radius of 15 μm. We further performed a dynamic characterization of the laser and realized a 6.5 GHz direct modulation without heat sinking. Integration of the directly modulated ring lasers on Si substrates with low threshold and high temperature operation looks promising.

Funding. Advanced Research Projects Agency–Energy (ARPA-E) (DE-AR0000672).

Acknowledgment. The authors would like to thank Prof. Kei May Lau, Di Liang, Chong Zhang, Minh Tran, Chao Xiang, Xinru Wu, and the UCSB nanofabrication clean room staff for helpful discussions and assistance.

†These authors contributed equally to this work.

REFERENCES

1. L. Ge, L. Feng, and H. G. L. Schwefel, "Optical microcavities: new understandings and developments," Photon. Res. **5**, OM1–OM3 (2017).
2. M. T. Hill and M. C. Gather, "Advances in small lasers," Nat. Photonics **8**, 908–918 (2014).
3. S. Longhi and L. Feng, "Unidirectional lasing in semiconductor microring lasers at an exceptional point [Invited]," Photon. Res. **5**, B1–B6 (2017).
4. T. Harayama, S. Sunada, and S. Shinohara, "Universal single-mode lasing in fully-chaotic two-dimensional microcavity lasers under continuous wave operation with large pumping power [Invited]," Photon. Res. **5**, B39–B46 (2017).
5. S. J. Herr, K. Buse, and I. Breunig, "LED-pumped whispering-gallery laser," Photon. Res. **5**, B34–B38 (2017).
6. J. Ma, X. Jiang, and M. Xiao, "Kerr frequency combs in large size, ultra-high-Q toroid microcavities with low repetition rates," Photon. Res. **5**, B54–B58 (2017).
7. Y. Han, Q. Li, S. Zhu, K. W. Ng, and K. M. Lau, "Continuous-wave lasing from InP/InGaAs nanoridges at telecommunication wavelengths," Appl. Phys. Lett. **111**, 212101 (2017).
8. Y. Shi, Z. Wang, J. V. Campenhout, M. Pantouvaki, W. Guo, B. Kunert, and D. V. Thourhout, "Optical pumped InGaAs/GaAs nanoridge laser epitaxially grown on a standard 300-mm Si wafer," Optica **4**, 1468–1473 (2017).
9. Z. Wang, B. Tian, M. Pantouvaki, W. Guo, P. Absil, J. Campenhout, C. Merckling, and D. Thourhout, "Room-temperature InP distributed feedback laser array directly grown on silicon," Nat. Photonics **9**, 837–842 (2015).
10. Y. Wan, Q. Li, A. Y. Liu, W. W. Chow, A. C. Gossard, J. E. Bowers, E. L. Hu, and K. M. Lau, "Sub-wavelength InAs quantum dot microdisk lasers epitaxially grown on exact Si (001) substrates," Appl. Phys. Lett. **108**, 221101 (2016).
11. N. Kryzhanovskaya, E. Moiseev, Y. Polubavkina, M. Maximov, M. Kulagina, S. Troshkov, Y. Zadiranov, Y. Guseva, A. Lipovskii, M. Tang, M. Liao, J. Wu, S. Chen, H. Liu, and A. Zhukov, "Heat-sink free CW operation of injection microdisk lasers grown on Si substrate with emission wavelength beyond 1.3 μm," Opt. Lett. **42**, 3319–3322 (2017).
12. Y. Wan, J. Norman, Q. Li, M. J. Kennedy, D. Liang, C. Zhang, D. Huang, A. Y. Liu, A. Torres, D. Jung, A. C. Gossard, E. L. Hu, K. M. Lau, and J. E. Bowers, "Sub-mA threshold 1.3 μm CW lasing from electrically pumped micro-rings grown on (001) Si," in *Proceedings of CLEO: Applications and Technology* (Optical Society of America, 2017), paper JTh5C.3.
13. S. A. Moore, L. O'Faolain, M. A. Cataluna, M. B. Flynn, M. V. Kotlyar, and T. F. Krauss, "Reduced surface sidewall recombination and diffusion in quantum-dot lasers," IEEE Photon. Technol. Lett. **18**, 1861–1863 (2006).
14. J. Gérard, O. Cabrol, and B. Sermage, "InAs quantum boxes: highly efficient radiative traps for light emitting devices on Si," Appl. Phys. Lett. **68**, 3123–3125 (1996).
15. J. Wang, H. Hu, C. Deng, Y. He, Q. Wang, X. Duan, Y. Huang, and X. Ren, "Defect reduction in GaAs/Si film with InAs quantum-dot dislocation filter grown by metalorganic chemical vapor deposition," Chin. Phys. B **24**, 028101 (2015).
16. M. Tang, S. Chen, J. Wu, Q. Jiang, K. Kennedy, P. Jurczak, M. Liao, R. Beanland, A. Seeds, and H. Liu, "Optimizations of defect filter layers for 1.3-μm InAs/GaAs quantum-dot lasers monolithically grown on Si substrates," IEEE J. Sel. Top. Quantum Electron. **22**, 50–56 (2016).
17. J. C. Norman, D. Jung, Y. Wan, and J. E. Bowers, "Perspective: the future of quantum dot photonic integrated circuits," APL Photon. **3**, 030901 (2018).
18. D. Bimberg and U. W. Pohl, "Quantum dots: promises and accomplishments," Mater. Today **14**, 388–397 (2011).
19. Z. Zhou, B. Yin, and J. Michel, "On-chip light sources for silicon photonics," Light Sci. Appl. **4**, e358 (2015).
20. S. Chen, W. Li, J. Wu, Q. Jiang, M. Tang, S. Shutts, S. Elliott, A. Sobiesierski, A. Seeds, I. Ross, P. Smowton, and H. Liu, "Electrically pumped continuous-wave III–V quantum dot lasers on silicon," Nat. Photonics **10**, 307–311 (2016).
21. D. Jung, Z. Zhang, J. Norman, R. Herrick, M. J. Kennedy, P. Patel, K. Turnlund, C. Jan, Y. Wan, A. C. Gossard, and J. E. Bowers, "Highly reliable low threshold InAs quantum dot lasers on on-axis (001) Si with 87% injection efficiency," ACS Photon. **5**, 1094–1100 (2017).
22. Y. Wan, J. Norman, Q. Li, M. J. Kennedy, D. Liang, C. Zhang, D. Huang, Z. Zhang, A. Y. Liu, A. Torres, D. Jung, A. C. Gossard, E. L. Hu, K. M. Lau, and J. E. Bowers, "1.3 μm submilliamp threshold quantum dot microlasers on Si," Optica **4**, 940–944 (2017).
23. Y. Wang, S. Chen, Y. Yu, L. Zhou, L. Liu, C. Yang, M. Liao, M. Tang, Z. Liu, J. Wu, W. Li, I. Ross, A. J. Seeds, H. Liu, and S. Yu, "Monolithic quantum-dot distributed feedback laser array on silicon," Optica **5**, 528–533 (2018).
24. J. Kwoen, B. Jang, J. Lee, T. Kageyama, K. Watanabe, and Y. Arakawa, "All MBE grown InAs/GaAs quantum dot lasers on on-axis Si (001)," Opt. Express **26**, 11568–11576 (2018).
25. J. Wang, H. Hu, H. Yin, Y. Bai, J. Li, X. Wei, Y. Liu, Y. Huang, X. Ren, and H. Liu, "1.3 μm InAs/GaAs quantum dot lasers on silicon with GaInP upper cladding layers," Photon. Res. **6**, 321–325 (2018).
26. S. Liu, D. Jung, J. Norman, M. Kennedy, A. Gossard, and J. Bowers, "490 fs pulse generation from passively mode-locked single section quantum dot laser directly grown on on-axis GaP/Si," Electron. Lett. **54**, 432–433 (2018).
27. D. Jung, J. Norman, M. J. Kennedy, C. Shang, B. Shin, Y. Wan, A. C. Gossard, and J. E. Bowers, "High efficiency low threshold current 1.3 μm InAs quantum dot lasers on on-axis (001) GaP/Si," Appl. Phys. Lett. **111**, 122107 (2017).
28. D. A. Miller, "Device requirements for optical interconnects to silicon chips," Proc. IEEE **97**, 1166–1185 (2009).
29. R. R. Alexander, D. T. Childs, H. Agarwal, K. M. Groom, H.-Y. Liu, M. Hopkinson, R. A. Hogg, M. Ishida, T. Yamamoto, M. Sugawara, Y. Arakawa, T. J. Badcock, R. J. Royce, and D. J. Mowbray, "Systematic study of the effects of modulation p-doping on 1.3-μm quantum-dot lasers," IEEE J. Quantum Electron. **43**, 1129–1139 (2007).
30. K. Otsubo, N. Hatori, M. Ishida, S. Okumura, T. Akiyama, Y. Nakata, H. Ebe, M. Sugawara, and Y. Arakawa, "Temperature-insensitive eye-opening under 10-Gb/s modulation of 1.3-μm p-doped quantum-dot lasers without current adjustments," Jpn. J. Appl. Phys. Part 2 **43**, L1124–L1126 (2004).
31. Y. Wan, Q. Li, A. Y. Liu, A. C. Gossard, J. E. Bowers, E. L. Hu, and K. M. Lau, "Temperature characteristics of epitaxially grown InAs quantum dot micro-disk lasers on silicon for on-chip light sources," Appl. Phys. Lett. **109**, 011104 (2016).
32. Y. Wan, J. Norman, D. Jung, C. Shang, L. Macfarlane, Q. Li, M. J. Kennedy, Z. Zhang, A. C. Gossard, E. L. Hu, K. M. Lau, and J. E. Bowers, "O-band electrically injected InAs quantum-dot

micro-ring lasers on V-groove patterned and unpatterned (001) silicon," Opt. Express **25**, 26853–26860 (2017).
33. O. B. Shchekin and D. G. Deppe, "Low-threshold high-to 1.3-μm InAs quantum-dot lasers due to P-type modulation doping of the active region," IEEE Photon. Technol. Lett. **14**, 1231–1233 (2002).
34. D. Jung, P. G. Callahan, B. Shin, K. Mukherjee, A. C. Gossard, and J. E. Bowers, "Low threading dislocation density GaAs growth on on-axis GaP/Si (001)," J. Appl. Phys. **122**, 225703 (2017).
35. A. Y. Liu, C. Zhang, A. Snyder, D. Lubyshev, J. M. Fastenau, A. W. Liu, A. C. Gossard, and J. E. Bowers, "MBE growth of P-doped 1.3 μm InAs quantum dot lasers on silicon," J. Vac. Sci. Technol. B **32**, 02C108 (2014).
36. R. L. Nagarajan, M. Ishikawa, T. Fukushima, R. S. Geels, and J. E. Bowers, "High speed quantum well lasers and carrier transport effects," IEEE J. Quantum Electron. **28**, 1990–2008 (1992).
37. D. Innoue, D. Jung, J. Norman, Y. Wan, N. Nishyama, S. Arai, A. C. Gossard, and J. E. Bowers, "Directly modulated 1.3 μm quantum dot lasers epitaxially grown on silicon," Opt. Express **26**, 7022–7033 (2018).
38. J. E. Bowers, B. R. Hemenway, A. H. Gnauck, and D. P. Wilt, "High-speed InGaAsP constricted-mesa lasers," IEEE J. Quantum Electron. **22**, 833–844 (1986).
39. T. Kageyama, Q. H. Vo, K. Watanabe, K. Takemasa, M. Sugawara, S. Iwamoto, and Y. Arakawa, "Large modulation bandwidth (13.1 GHz) of 1.3 μm-range quantum dot lasers with high dot density and thin barrier layer," in *Proceedings of the Compound Semiconductor Week (CSW'2016)* (2016), paper MoC3–4.
40. D. Arsenijević and D. Bimberg, "Quantum-dot lasers for 35 Gbit/s pulse-amplitude modulation and 160 Gbit/s differential quadrature phase-shift keying," Proc. SPIE **9892**, 98920S (2016).